On the Phase Transitions in Ammonium Hexafluoroaluminate(III)

Keiichi MORIYA,* Takasuke MATSUO, Hiroshi SUGA, and Syûzô SEKI
Department of Chemistry, Faculty of Science, Osaka University, Toyonaka Osaka 560

(Received January 5, 1979)

The heat capacities of $(NH_4)_3[AlF_6]$ were measured between 11 and 300 K with an adiabatic calorimeter. Two anomalies were found at (193.0±0.3) K and (220.79±0.05) K. The enthalpy and entropy of the phase transitions are (790±150) J mol^{-1} and (4.2±0.8) J K^{-1} mol^{-1} for the former, and (4030±150) J mol^{-1} and (18.5±0.7) J K^{-1} mol^{-1} for the latter, respectively. The total anomalous entropy, (22.7±1.5) J K^{-1} mol^{-1}, is in agreement with R ln 16=23.05 J K^{-1} mol^{-1} predicted by a model involving orientational disorder of the hexafluoroaluminate(III) and the ammonium ions. Discontinuities in fluorine T_1 and $T_{1\rho}$ at 221 K by pulse NMR measurement also support this model. The potential barrier height of the hindered rotation of the NH_4^+ ion was estimated to be 7 kJ mol^{-1} from the heat capacity data. The intermediate phase undercooled and coexisted with the low temperature phase in a limited range of temperature. The upper phase transition is of the first order but the anomalous heat capacity follows the Landau theory of the phase transitions of the second kind. The high symmetry of the crystal structure of the present crystal at room temperatures in comparison with that of the alkali cryolites was discussed in terms of the hydrogen bonding, molecular disorder and packing consideration.

There is currently a considerable interest in the phase transitions of crystals containing $[AX_6]^{n-}$ ions, where A is a multivalent atom and X halogen. The phase transitions hitherto studied of this type of compound appear to be displacive if X is chlorine, *e.g.*, $K_2[SnCl_6]$,[1,2] $(NH_4)_2[SnCl_6]$,[3] $K_2[ReCl_6]$,[4] $K_2[OsCl_6]$,[4] and $(NH_3CH_3)_2[SnCl_6]$.[5] Spectroscopic studies have shown that low-frequency rotational vibrations of $[ACl_6]^{2-}$ ion play an important role in the phase transitions in these crystals.[2,3,5] The entropy of transition, in case where calorimetric data are available, is relatively small in agreement with the displacive mechanism of the transitions. For X= fluorine, we have shown that the phase transition is of order-disorder type in $(NH_4)_3[FeF_6]$ crystal.[6] The large entropy of transition ($\Delta S \simeq 24.8$ J K^{-1} mol^{-1}) was accounted for in terms of a model involving orientational disorder of both the ammonium and hexafluoroferrate (III) ions. It was pointed out that the same orientational disorder explains, albeit qualitatively, why ammonium hexafluoroferrate(III) crystal is cubic at room temperature while alkali hexafluoroferrates(III) are not.

In the present paper we will report a calorimetric and NMR study of phase transitions in ammonium hexafluoroaluminate (ammonium cryolite), $(NH_4)_3[AlF_6]$. It will be shown that this crystal is very similar to ammonium hexafluoroferrate(III) in regard to the ionic disorder but the low temperature behavior, having an additional phase transition, is more complicated than in the iron compound.

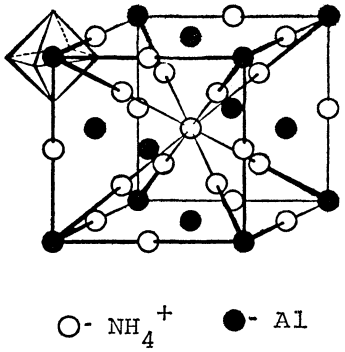

Fig. 1. Crystal structure of $(NH_4)_3[AlF_6]$.

$(NH_4)_3[AlF_6]$ at room temperature is isomorphous with cubic $(NH_4)_3[FeF_6]$. The structure[7] is illustrated in Fig. 1. The aluminum atoms occupy the corner (0,0,0) and face-center (1/2,1/2,0) of the cube. The fluorines are placed tentatively on the four-fold axis of the crystal to form a regular octahedron around the aluminum. There are two sites for the ammonium ions. One is on the edge of the cube (1/2,0,0) and the other (1/4,1/4,1/4). There are four of the former in the unit cell of the fcc Bravais lattice and eight of the latter.

The crystal is not cubic at 93 K. Steward and Rooksby[7] called it pseudo tetragonal. Schwarzmann[8] found that $(NH_4)_3[InF_6]$ belongs to the monoclinic system (C_{2h}^5-$P2_1/n$) and that $(NH_4)_3[AlF_6]$ undergoes a phase transition at 224 K which he described as displacive. Thus it has been known that there is a phase transition between the room temperature and 93 K. It will be shown below that there are in fact two phase transitions.

Comparison of the crystal structure of alkali and ammonium hexafluoroaluminates and analogous hexafluoroferrates(III) shows that there is similar behavior as the size of cation increases in these two families. In Table 1[9] which summarizes the crystal system and the molar volume of the cryolite family, it is shown that smaller alkali cations excluding lithium tend to form less symmetric crystals. The molar volume of the ammonium cryolite is intermediate between those of Rb and Cs compounds. The fcc symmetry of the ammonium cryolite is thus anomalously high in

Table 1. The crystal system and molar volume of cryolite-type compounds $A(I)_3[AlF_6]$ at room temperature

A(I)	Crystal system	Molar volume / cm^3 mol^{-1}
Li	orthorhombic	58.9
Na	monoclinic	72.0
K	tetragonal	90.4
Rb	tetragonal	102.0
Cs	tetragonal	117.4
NH_4	cubic	107.2

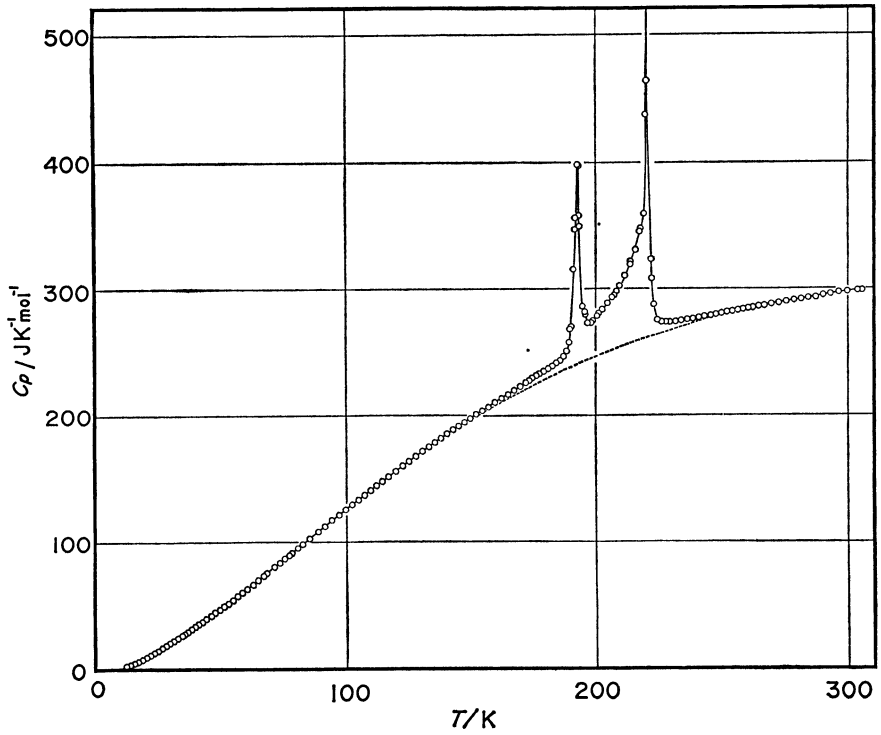

Fig. 2. Molar heat capacity of $(NH_4)_3[AlF_6]$.

this family. It will be shown below that the anomalous property of the ammonium compound is closely related to the orientational disorder and packing of the ions.

Experimental

Sample Preparation. Metallic aluminum of stated 99.99% purity was dissolved in extra-pure reagent of hydrofluoric acid (Wako Pure Chemical Industries, Ltd.). The aluminum fluoride solution thus prepared was added to the aqueous solution of the 1.5 times equivalent amount of extra-pure reagent of ammonium fluoride (Wako Pure Chemical Industries, Ltd.). The reaction was performed at 60 °C. The precipitated crystal, $(NH_4)_3[AlF_6]$, was repeatedly digested at 90 °C. The crystal obtained was separated by filtration, washed with methanol and dried *in vacuo* at 90 °C. Polyethylene or teflon laboratory ware was used exclusively throughout the sample preparation. The crystal was kept in an evacuated desiccator together with calcium oxide before heat capacity measurement. The elemental analysis was made by oxine gravimetric method for Al, by thorium nitrate titration for F and gravimetric method for N and H. The values given below in parentheses are calculated for the chemical formula $(NH_4)_3[AlF_6]$; Al: 13.80±0.04 (13.83%), F: 58.3±0.4 (58.5%), H: 6.17± 0.20 (6.20%), N: 21.3±0.2 (21.54%).

Differential Thermal Analysis and X-Ray Powder Photograph. The thermal behavior was first examined by differential thermal analysis (DTA).[10] Only one exothermic peak was detected at 220 K on cooling at the rate of 3 K/min down to 100 K. On the other hand two peaks were observed in the heating run around 190 K and 220 K, respectively. This behavior was reproducible with the same crystal. X-Ray powder photographs taken at 125, 216 and 293 K gave different diffraction patterns. The pattern at 293 K was fully indexed with the fcc lattice. The intermediate and the lowest-temperature patterns were increasingly complicated and could not be indexed. However, by the DTA and the Debye-photograph data it became evident for the first time that ammonium hexafluoroaluminate is trimorphic below the room temperature. The hysteresis phenomenon in DTA was confirmed in the heat capacity measurement as will be discribed below.

Heat Capacity Measurement. The heat capacity was measured from 11 K to 300 K with an adiabatic calorimeter. The calorimeter consists of the sample cell and double adiabatic jackets surrounding it. They are suspended in a vacuum chamber. The temperature of the cell was measured with a platinum resistance thermometer calibrated in terms of the IPTS-68. Precision of the heat capacity measurement was ±0.05% in the temperature range above 50 K, and the estimated accuracy ±1% at 20 K and 0.1% above 50 K. Details of the construction of the calorimeter were published elsewhere.[11]

The calorimeter cell, a chromium plated thin-walled copper cylinder with the thermometer and heater, was loaded with 44.296 g (0.22706 mol) of the $(NH_4)_3[AlF_6]$ crystal, evacuated to approximately 1 Pa, filled with 10^5 Pa of He gas at 20 °C and then sealed off with low melting solder. The increment of the temperature in one measurement of the heat capacity was 1—3 K in the normal temperature region and less than 0.1 K in the transition region. The experimental heat capacity values are given in Table 2 and shown in Fig. 2. Two heat capacity peaks were found at (193.0± 0.3) K and (220.79±0.05) K, respectively. These temperatures agree well with the DTA result. The high temperature anomaly has a premonitory effect already at 193 K where the peak height of the low temperature anomaly reaches maximum. The apparent heat capacity reached 23000 J K^{-1} mol^{-1} at the upper phase transition. The time required for thermal equilibration in the neighbourhood of both phase transitions increased to about an hour, compared with ten minutes normally required in normal region. Such a behavior is often observed in the first order transitions. Figure 3 shows the cooling curve obtained by slow removal

Table 2. Heat capacity of $(NH_4)_3AlF_6$

T_{av}/K	C_p/J K^{-1} mol^{-1}	T_{av}/K	C_p/J K^{-1} mol^{-1}	T_{av}/K	C_p/J K^{-1} mol^{-1}	T_{av}/K	C_p/J K^{-1} mol^{-1}
1 st series		65.60	71.53	200.49	278.5	198.64	274.7
11.99	2.13	68.35	75.84	202.82	283.8	199.76	276.9
13.07	2.77	71.11	80.08	205.12	289.6	201.47	280.3
13.93	3.38	73.43	83.73	207.38	295.4	203.07	284.4
14.65	3.93	75.64	87.27	209.60	302.2	204.90	288.9
15.41	4.55	78.20	91.37	211.78	310.5	206.52	293.2
16.20	5.18	80.66	95.35	213.91	319.8	208.19	298.1
16.96	5.93	3 rd series		215.99	331.7	210.16	303.9
17.77	6.71	80.15	94.56	217.99	347.7	212.10	311.9
18.58	7.51	82.52	98.46	219.81	437.1	213.98	320.9
19.38	8.38	85.28	102.9	220.69	7349	215.85	330.4
20.19	9.29	88.57	108.1	220.78	23300	217.66	345.1
20.96	10.26	91.47	112.8	221.10	1378	219.12	359.9
21.76	10.87	94.31	117.1	222.48	308.2	220.16	464.5
22.56	11.95	97.10	121.6	224.72	274.5	220.68	5605
23.30	12.77	99.81	125.7	227.06	273.2	220.75	15540
24.09	13.74	102.38	129.7	229.40	273.3	220.78	22050
24.94	14.68	104.92	133.6	231.73	273.7	220.80	23130
25.72	15.67	107.38	137.3	234.05	274.4	221.07	963.3
26.46	16.49	109.79	141.0	236.37	275.1	221.94	323.5
27.18	17.40	112.14	144.5	238.68	275.8	223.23	287.3
27.93	18.30	114.44	148.0	240.98	276.8	224.60	275.0
28.76	19.35	117.00	151.7	243.27	277.5	226.17	273.6
29.55	20.34	119.80	156.0	245.56	278.4	228.08	273.4
30.29	21.17	122.54	160.4	247.83	279.1	230.17	273.5
31.09	22.16	125.22	159.9	250.03	279.9	5 th series	
31.93	23.29	127.86	167.7	252.23	281.0	262.52	284.6
32.73	24.36	130.46	171.3	254.48	281.5	264.75	285.6
33.57	25.39	133.02	174.9	256.73	282.8	267.15	286.2
34.44	26.52	135.51	178.4	258.96	283.5	269.91	287.8
35.44	27.86	137.97	181.7	261.18	284.0	272.85	288.0
36.79	29.67	140.38	185.1	4 th series		275.78	289.2
38.27	31.57	142.76	188.3	172.07	225.6	278.70	290.3
39.66	33.45	145.11	191.4	173.50	227.5	281.60	291.2
41.07	35.29	147.42	194.4	174.91	229.1	284.49	292.4
42.46	37.08	149.70	197.5	176.32	231.0	287.39	292.9
44.08	39.37	152.12	200.9	177.73	232.5	290.28	294.3
45.97	41.91	154.60	203.7	179.29	234.5	293.22	295.0
47.65	44.38	157.08	206.9	181.02	236.3	296.37	295.9
49.39	46.91	159.69	210.2	182.73	238.8	299.83	297.0
51.17	49.52	162.27	213.5	184.35	241.1	6 th series	
52.92	51.09	164.80	216.7	185.78	243.1	187.49	254.8
54.66	54.67	167.32	219.9	187.15	246.1	188.69	255.9
56.61	57.44	169.81	222.8	188.34	250.2	190.05	258.8
58.38	60.30	172.26	226.0	189.32	257.2	191.57	261.4
60.33	63.34	174.69	229.0	190.27	269.9	193.27	264.3
62.69	66.73	177.09	231.8	191.15	315.6	195.12	267.9
64.67	70.14	179.47	235.0	191.95	356.1	197.10	271.7
66.81	73.51	181.92	237.9	192.68	398.7	199.15	275.8
71.33	80.47	184.42	241.2	193.38	397.6	201.08	280.2
75.47	87.10	187.37	247.0	194.11	358.3	203.08	284.6
77.15	89.66	189.39	268.0	194.88	285.9	7 th series	
79.13	92.91	191.61	346.9	195.83	279.8	181.59	244.5
81.04	96.05	193.59	349.8	196.75	272.6	182.88	246.5
2 nd series		195.76	281.7	197.67	272.8	184.53	249.6
62.66	66.98	198.13	272.9			186.30	252.0

Table 2. Continued.

T_{av}/K	C_p/J K^{-1} mol^{-1}	T_{av}/K	C_p/J K^{-1} mol^{-1}
188.05	255.3	190.74	282.4
189.96	258.8	192.67	313.7
192.01	265.9	194.64	278.9
194.03	267.9	196.71	271.1
196.04	269.5	198.77	275.1
198.03	273.5	200.82	279.3
199.97	277.5	9 th series	
201.91	281.8	175.52	231.1
8 th series		176.93	232.9
174.61	232.4	178.31	235.3
176.26	234.1	179.68	236.4
178.39	237.4	181.04	238.6
180.50	240.2	182.39	240.4
182.59	243.2	184.08	242.9
184.68	246.4	186.09	246.2
186.70	250.4	188.06	252.3
188.75	256.4	189.67	266.2

of heat from the specimen. The cooling rate 0.7 K/h at the normal region was effected by introduction of an appropriate back-up potential in the cell-jacket thermocouple circuit. The temperature arrest occurred at (220.79±0.05) K which was in good agreement with the temperature of the heat capacity peak. No temperature halt was observed, however, at the lower temperature where the low temperature transition was expected to occur. This is consistent with the DTA result that the low temperature anomaly is observed only in the heating run. The hysteresis was then studied by the heat capacity measurement. The crystal was first cooled down to 186.8 K, 6.2 K below the lower transition temperature. Subsequent measurement of the heat capacity gave the curve that joins smoothly to the heat capacity of the intermediate phase, as shown by the Series 2 curve in Fig. 4. The crystal was cooled then to 180.9 K and again the heat capacity was measured, giving the Series 3 curve. There occurred a small anomaly at 193.0 K in this series. Similar series of measurements after precooling to increasingly lower temperatures gave Series 4 (173.9 K)- and 5 (171.3 K)- curves in Fig. 4, respectively. In these measurements, the temperature drift was less than the observational limit, 0.1 mK h^{-1}. It is therefore concluded that the two phases (the intermediate and the low temperature phases) coexist side by side indefinitely in the temperature range between 193.0 K and the temperature of the precooling. The heat capacity values above 80.15 K plotted in Fig. 2 and given as the 3rd series in Table 2 pertain to the crystal cooled to 78 K and are believed to represent the crystal fully converted to the low temperature phase.

Thermodynamic Quantities. The tempered enthalpy, entropy and heat capacity of $(NH_4)_3[AlF_6]$ crystal are given in Table 3. These values refer to the stabilized crystal.

The Proton and Fluorine Nuclear Relaxation Times.† The

† More detailed NMR study was presented at the Symposium on Molecular Structures and Molecular Electronic States, Tokyo, 1976 (Title: "Nuclear magnetic relaxation and molecular motion of ^{1}H, ^{19}F, ^{27}Al in $(NH_4)_3[AlF_6]$" by Yoshihiro Furukawa, Hideko Kiriyama, Keiichi Moriya and Takasuke Matsuo).

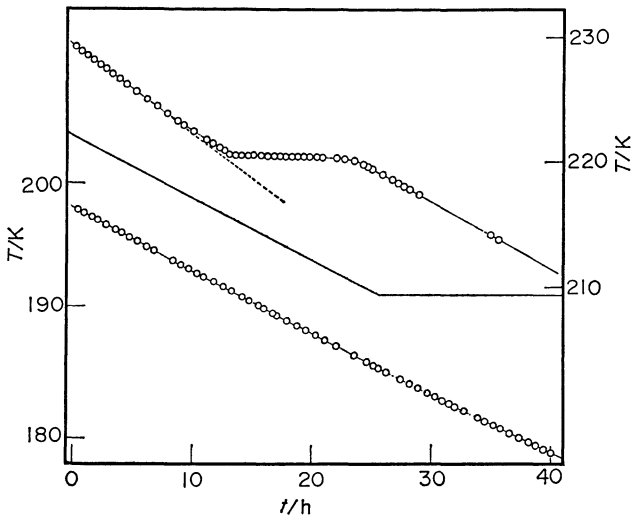

Fig. 3. Cooling curve of $(NH_4)_3[AlF_6]$.

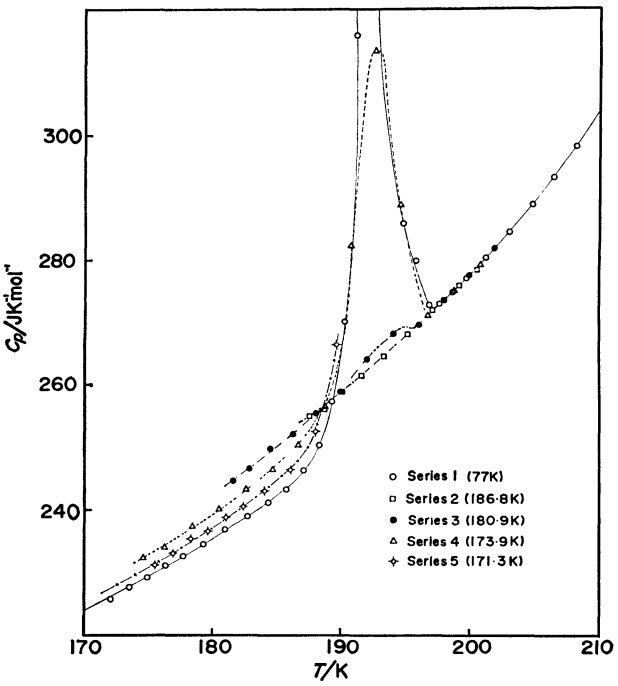

Fig. 4. Hysteresis phenomenon of the heat capacity of $(NH_4)_3[AlF_6]$ around the lower phase transition.

spin relaxation time T_1 was measured for the proton and fluorine nucleus by use of a pulse NMR spectrometer, Brucker Model BK-322S, in the temperature range between 15 and 350 K. The T_1 was measured at 60 and 20 MHz by the 180°-τ-90° method, and, at lower temperatures, by the 90°-τ-90° method. $T_{1\rho}$ in the rotating frame was also measured by the method of Look *et al.*[12] The powder sample was sealed in a thin-wall glass ampule of 5 mm diameter together with He gas. The sample temperature was measured with either a copper-constantan or copper cobalt-doped-gold thermocouples, depending on the temperature region. The temperature was stabilized at least 30 min in each of the measurements.

The T_1 and $T_{1\rho}$ for the proton are shown in Fig. 5. On cooling the crystal from the room temperature, T_1 decreased gradually and underwent a jump at 222 K to a lower value. The gradually decreasing portion of the curve was fitted to the Arrhenius equation and gave an activation enthalpy

Table 3. Thermodynamic function of $(NH_4)_3[AlF_6]$

T / K	C_p° / J K^{-1} mol^{-1}	$S^\circ - S_0^\circ$ / J K^{-1} mol^{-1}	$[H^\circ - H_0^\circ]/T$ / J K^{-1} mol^{-1}	$-[G^\circ - H_0^\circ]/T$ / J K^{-1} mol^{-1}
10	(1.24)	(0.30)	(0.31)	(0.10)
20	9.04	3.23	2.41	0.83
30	20.85	9.09	6.55	2.54
40	33.80	16.83	11.22	5.11
50	47.79	25.81	17.47	8.34
60	62.75	35.84	23.76	12.08
70	78.40	46.69	30.45	16.24
80	94.30	58.19	37.43	20.76
90	110.3	70.22	44.65	25.58
100	126.0	82.67	52.00	30.66
110	141.2	95.39	59.43	35.97
120	156.1	108.3	66.87	41.45
130	170.7	121.4	74.30	47.10
140	184.6	134.6	81.69	52.87
150	198.0	147.8	88.99	58.77
160	210.6	160.9	96.20	64.74
170	223.1	174.1	103.3	70.79
180	235.6	187.2	110.3	76.89
190	265.2	200.4	117.3	83.04
200	277.6	216.2	126.9	89.30
210	303.5	230.3	134.6	95.68
220	441.0	245.7	143.6	102.1
230	273.5	270.0	160.8	109.2
240	276.3	281.6	165.6	116.1
250	279.9	293.0	170.1	122.9
260	283.8	304.1	174.4	129.7
270	287.4	314.8	178.5	136.4
280	290.9	325.3	182.4	142.9
290	294.2	335.6	186.2	149.4
300	297.1	345.6	189.9	155.8
273.15	288.5	318.2	179.7	138.4
298.15	296.6	343.8	189.2	154.6

of 14.6 kJ mol^{-1}. The T_1 at 20 MHz reached the maximum value at approximately 357 K, indicating onset of another relaxation mechanism operating at higher temperature. The same relaxation mechanism showed itself in $T_{1\rho}$ which reached the maximum value at 250 K and decreased with the increasing temperature. The activation enthalpy derived from the $T_{1\rho}$ is 22.5 kJ mol^{-1}. This is assigned tentatively to diffusional motion of the ammonium ion, as the AC conductivity[13] increased rapidly above the room temperature.

In the intermediate phase, a T_1 minimum of the proton of 5.4 ms occurred at (200±2) K for $\omega_0/2\pi=20$ MHz. The corresponding T_1 minimum for $\omega_0/2\pi=60$ MHz, as calculated by the BPP equation, will be 16.2 ms and may be identified with the experimental value of 16.2 ms at (213±2) K.

The T_1 value shows a hysteresis at the lower transition consistently with the calorimetric observations. The cooling run gave slightly larger T_1. Below 200 K, T_1 remained more or less constant down to 78 K with shallow minima in the T_1 *vs.* $1/T$ curve. In the temperature range from 111 to 197 K, slight deviation from the exponential law was observed in the magnetization *vs.* τ curve. This may be reasonable in view of the presence of the proton and fluorine nuclei in the crystal. It was not possible, however, to evaluate separately the two T_1 values characterizing the cross relaxations. The values plotted in Fig. 5 are those of the faster relaxation process.

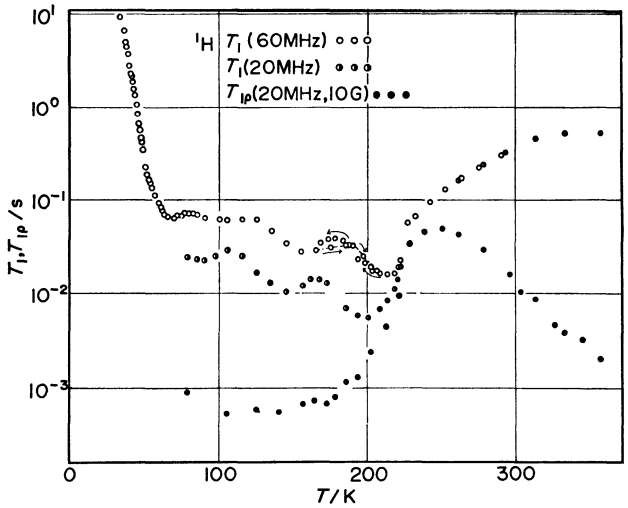

Fig. 5. Proton T_1 and $T_{1\rho}$ in $(NH_4)_3[AlF_6]$, plotted semi-logarithmically against temperature.

The temperature dependence of the fluorine T_1 (Fig. 6) is similar to that of the proton. In the high temperature phase, the T_1 at 20 MHz and 60 MHz are the same at least to 291 K. It increased with the increasing temperature,

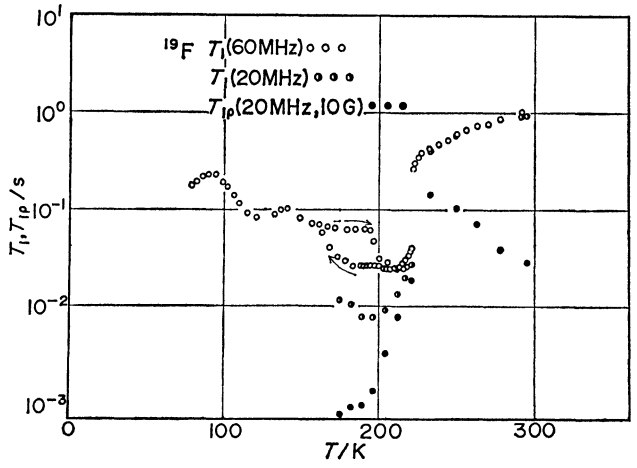

Fig. 6. Fluorine T_1 and $T_{1\rho}$ in $(NH_4)_3[AlF_6]$, plotted semi-logarithmically against temperature.

while the $T_{1\rho}$ measured at $H_1=10$ G decreased with the increasing temperature. There is a large jump of the fluorine T_1 at the upper transition temperature. The ratio of the T_1 of the high temperature phase to that of the intermediate phase at the transition temperature is four times as large for the fluorine resonance as for the proton. A T_1 minimum of 8.7 ms for 20 MHz occurred at (193±2) K. This value pertains to the intermediate phase because the data was taken in a cooling run. A hysteresis behavior was found again around the intermediate-to-the-low-temperature phase transition. The difference in the T_1 values obtained in the cooling and heating runs is larger for the fluorine resonance than for the proton.

Discussion

Heat Capacity of the High Temperature Phase. One does not expect that the heat capacity of a complex compound should be equal to the sum of the heat capacities of the components of the compound. However, approximate equality holds between the heat capacity of an alloy and that of the component metals and is known as the Neumann-Kopp law. We have examined the validity of the additivity of the heat capacity of the hexafluoroaluminates as shown in Fig. 7 where the difference (ΔC_p) between the experimental value and the Neumann-Kopp sum are plotted in ordinate. The heat capacity data were taken from Furukawa, Saba and Ford ($Li_3[AlF_6]$)[14], Clusius, Goldmann and Perlick (LiF)[15], and King ($Na_3[AlF_6]$, NaF, and AlF_3)[16]. ΔC_p is very small for these hexafluoroaluminates between 220 and 300 K considering that the total heat capacity amounts to 200 J K^{-1} mol^{-1} of $M_3[AlF_6]$, although the fractional difference increases with the decreasing temperature at lower temperature as Furukawa, Saba and Ford noted. Similar calculation was done for the high temperature phase of $(NH_4)_3[AlF_6]$ by using the present heat capacity data and those by Benjamins and Westrum (NH_4F)[17] and King (AlF_3)[16]. There is a large positive deviation from the Neumann-Kopp law as shown in Fig. 7. The internal vibrations of the $[AlF_6]^{3-}$ and NH_4^+ ions are practically independent of their environment as far as their contribution to the heat capacity is

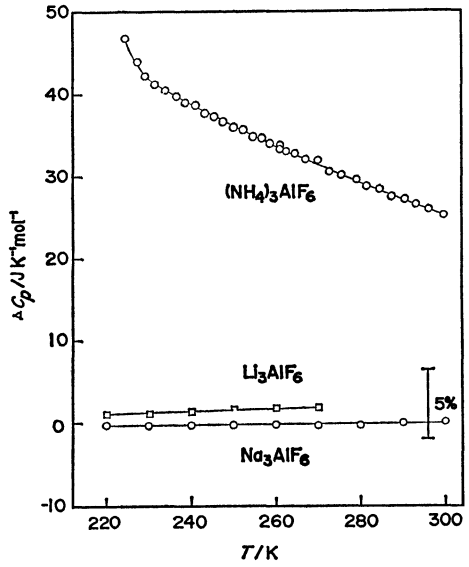

Fig. 7. Additivity of the heat capacity of hexafluoroaluminates.
$3C_p(3M(I)F)+C_p(AlF_3)=C_p(M(I)_3[AlF_6])$

concerned. One may, therefore, attribute the positive deviation from the Neumann-Kopp law to the difference in the external vibrations of the ammonium ions in NH_4F and $(NH_4)_3[AlF_6]$. There are two types of the external vibrations, translational and rotational. Translational vibrations of the cation are involved also in $Li_3[AlF_6]$ and $Na_3[AlF_6]$. But the Neumann-Kopp law holds to a good approximation for these substances. Therefore, the rotational motion of the ammonium ions is responsible to the non-additivity of the heat capacity. It is very reasonable to assume that the rotational motion of the ammonium ion is much more hindered in NH_4F than in $(NH_4)_3[AlF_6]$ in view of the strong NH···F hydrogen bonding in the former crystal[18]. The fluorine atoms in fluorocomplex ions such as $[SiF_6]^{2-}$, $[PF_6]^-$ and $[BF_4]^-$ are generally poor hydrogen-bond acceptors in comparison with the fluoride ion F^-, as is evident from the higher N–H stretching frequencies in these compounds.[19–21]

An estimate of the rotational heat capacity of NH_4^+ ion in $(NH_4)_3[AlF_6]$ crystal is obtained by addition of three times the rotational heat capacity of the ammonium ion in NH_4F to the heat capacity difference given in Fig. 7. The former is calculated by the harmonic approximation by using the three-fold degenerate frequency of 523 cm^{-1}.[18] The result of the calculation for the present crystal is plotted in Fig. 8 (data designated by (B)) for one mole of NH_4^+ ion.

A slightly different estimate of the rotational heat capacity is obtained by subtraction of the heat capacity of $Na_3[AlF_6]$ from that of $(NH_4)_3[AlF_6]$ and making a small correction for the internal vibration of the ammonium ion. This is equivalent to assuming that all the translational vibrations and the internal vibrations and rotational parts of the external vibrations of the $[AlF_6]^{3-}$ anion in $(NH_4)_3[AlF_6]$ crystal are the same as the corresponding vibrations in $Na_3[AlF_6]$ crystal, as far as their contributions to the heat capacity are concerned. The difference between the C_p and

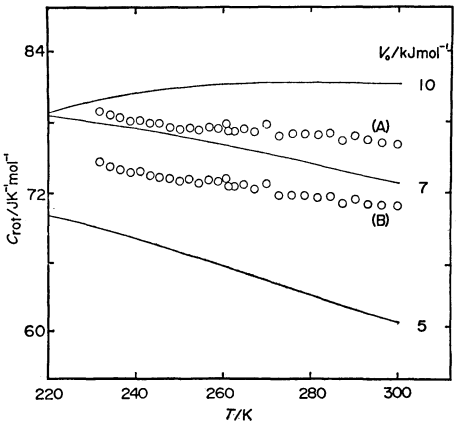

Fig. 8. NH_4^+ ion rotational heat capacity in $(NH_4)_3[AlF_6]$ by two methods
(A) $C_{rot}=C((NH_4)_3[AlF_6])-C(Na_3[AlF_6])-3C(NH_4^+$ internal).
(B) $C_{rot}=C((NH_4)_3[AlF_6])-C(AlF_3)-3C(NH_4F)+9C$(Harmonic, $\sigma=523$ cm^{-1}).

C_v is also assumed to cancel out by the subtraction. The estimated rotational heat capacity is plotted also in Fig. 8 as data (A). Accuracy of the assumptions made here is difficult to assess. But the good agreement of two independent estimates (difference 7%) indicates the essential correctness of the derived rotational heat capacity. The derived value is approximately equal to the heat capacity of three harmonic oscillators in the classical limit. However, it decreases with increasing temperature. This behavior is often observed in a high-temperature heat capacity of a hindered rotator. In Fig. 8, approximate calculations for the hindered rotational heat capacity are plotted for the hindering potential V_0 of 5, 7 and 10 kJ mol^{-1}. The calculation with $V_0=7$ kJ mol^{-1} reproduces fairly well the experimental heat capacity. Here, three dimensional rotation of the ion was approximated as the sum of one dimensional rotations[22] and the two ammonium ions at (1/2,0,0) and at (1/4, 1/4,1/4) were assumed to have the same heat capacity. In spite of these limitation one may conclude that the barrier hindering the rotation of the ammonium ion is much lower in $(NH_4)_3[AlF_6]$ than in NH_4F[23] for which the barrier height of 42 kJ mol^{-1} was reported. This may be another instance of a general observation that fluorocomplex ions are poor hydrogen-bond acceptors.

The activation enthalpy derived from the T_1 measurement, 14.6 kJ mol^{-1} differs from the calorimetric barrier height. Quantitative comparison of the two values will be justified when quantum mechanical calculation of three dimensional motion[24] of the ion is performed for the present compound.

Ionic Motion in the Intermediate and Low Temperature Phases. The T_1 minimum of the proton for $\omega_0/2\pi=20$ MHz indicates that the correlation time of the reorientational motion of the ammonium ion is 4.9 ns at (200±2) K. The activation enthalpy from the temperature dependence of T_1 near the minimum is ≈23 kJ mol^{-1} and the pre-exponential factor of the correlation time τ_0 4.8 fs. An approximately equal value is obtained from the T_1 value at 60 MHz. The minimum value of T_1, 5.4 ms, at 20 MHz is comparable with 3.1—4.3 ms calculated for a reasonable range of the proton–proton distance in ammonium ion by use of the BPP mechanism involving random reorientation of the ion.[25,26] The second moment of the proton resonance absorption is 5.4 G^2 in the intermediate phase[27] and supports the rapid reorientation model. In the calculation of the T_1 minimum all of the ammonium ions are assumed to have the same correlation time. The fair agreement of the experimental and calculated values appears to support this simplification. The relatively short T_1 found in the low temperature phase suggests the occurrence of some reorientational motion of the ammonium ions in this phase. However, detailed interpretation of the shallow T_1 minima is not possible at present because of lack of the structural information.

The T_1 minimum of 8.7 ms of the fluorine resonance occurs in the intermediate phase for $\omega_0/2\pi=20$ MHz. The activation enthalpy derived from the fluorine T_1 is 23 kJ mol^{-1} and equal to that derived from the proton T_1. This suggests that the same mechanism (reorientation of NH_4^+) is involved in the proton and fluorine relaxations, though reorientation of hexafluoroaluminate ion cannot be ruled out. In the cubic $(NH_4)_2[SiF_6]$, reorientation of $[SiF_6]^{2-}$ octahedron begins to take part in the fluorine relaxation above 360 K and the fluorine second moments retains its rigid lattice value up to 300 K.[28] On the other hand, fluorine T_1 minimum occurs in the temperature range 130—245 K for the low temperature phase of $Na[PF_6]$, $K[PF_6]$ and $Rb[PF_6]$.[29] These minima are caused by reorientation of the fluorine octahedron. In $NH_4[PF_6]$ both proton and fluorine T_1's show minima due to the reorientation of $[PF_6]^-$[30] at 125 K. The second moment of the fluorine resonance of $(NH_4)_3[AlF_6]$ is 3.1 G^2 in the intermediate phase.[23] It is evident that the $[AlF_6]^{3-}$ ion reorients rapidly and that the same motion can well contribute to the nuclear relaxation at some appropriate temperature. T_1 measurements of $(ND_4)_3[AlF_6]$ will be interesting in this respect. This will disentangle the probable complication arising from the motion of ammonium and hexafluoroaluminate ions and cross relaxation through the interaction of the proton and fluorine.

Increase of the proton T_1 in the temperature range 30—50 K gives an activation enthalpy of 2.5—3 kJ mol^{-1}. It is not clear if this really corresponds to a potential barrier hindering another reorientational motion of the ammonium ion. Effect of the tunnelling motion of the ammonium ion is excluded because the second moment of the proton resonance increases toward the rigid lattice value around 80 K[27] and the T_1 value becomes very high (≈100 s) at 15.8 K. Interestingly, the activation energy corresponds to 210—250 cm^{-1} of the wave number or the frequency of typical optical lattice vibration of translational or rotational origin. Physical implication of the coincidence of these two energy parameters is not clear at present.

Mechanism of the Phase Transitions. The enthalpy and entropy of the phase transitons were evaluated

Table 4. "Normal" heat capacity of $(NH_4)_3AlF_6$

T/K	C_p/J K^{-1} mol^{-1}	T/K	C_p/J K^{-1} mol^{-1}
150	196.5	210	254.4
160	207.9	220	261.6
170	218.7	230	268.0
180	228.7	240	273.8
190	237.9	250	279.2
200	246.5	260	283.6

Table 5. Phase transitions of $(NH_4)_3[AlF_6]$

T/K	ΔH/J mol^{-1}	ΔS/J K^{-1} mol^{-1}
193.0 ±0.3	790±150	4.2±0.8
220.79±0.05	4030±150	18.5±0.7

by integrating the excess heat capacity over the normal value. The normal heat capacity was determined by smooth interpolation of the low and the high temperature heat capacities into the anomalous region. The normal heat capacity employed here is given in Table 4. The entropies and enthalpies of both transitions are given in Table 5.

If one assumes that the orientation of the ions is uniquely fixed in the low temperature phase, the entropy of transition ΔS is related to the number W of different orientations allowed to the ions in the high temperature phase through the equation, $\Delta S = R \ln W$, provided that the vibrational entropy is adequately taken into account by the lattice heat capacity. The sum of the entropies of the two transitions (22.7± 1.5) J K^{-1} mol^{-1} corresponds to $W=15.3\pm3.0$. An approximately equal value was found for the entropy of transition in $(NH_4)_3[FeF_6]$.[6] One interpretation of $W=16$ is to ascribe it entirely to the disorder of the ammonium ion. $[AlF_6]^{3-}$ ion having the O_h symmetry occupies the site of O_h symmetry, the (0,0,0) position in the fcc Bravais lattice, and is assumed to have uniquely fixed orientation. There are two types of the ammonium ions, one in the (1/2,0,0) position and the other in the (1/4,1/4,1/4). One formula unit of $(NH_4)_3[AlF_6]$ contains one of the former ammonium and two of the latter. The experimental transition entropy may be interpreted formally by allowing four orientations to each of the former ammonium and two to the latter, or $W=4\times2\times2=16$. However, four equivalent orientations of the NH_4^+ ion in the (1/2, 0,0) position is inconceivable from the geometrical viewpoint. Moreover, absence of phase transitions in the cubic $(NH_4)_2[SiF_6]$ disfavors this model. In the cubic $(NH_4)_2[SiF_6]$, the ammonium ions are all equivalent and occupy the (1/4,1/4,1/4) positions. In this case the site symmetry is T_d so that the ammonium ions occupy the site without two-fold disorder. As will be discussed below, the ammonium ion in the (1/4,1/4,1/4) position appears to stabilize the cubic structure energetically. Another interpretation of $W=16$ proposed earlier[6] will be appropriate to the present crystal also. It involves orientational disorder of the $[AlF_6]^{3-}$ ion. Because of the O_h symmetry of the Al site, the orientational disorder has to be one-fold (ordered) or eight-fold. The latter corresponds to rigid rotation of the fluorine octahedron which shifts the fluorine atom from $(x,0,0)$ to a general position. There are eight different orientations of this type.[6] Allowing two orientations to the (1/2,0,0) ammonium in conformity with the site (O_h) and ionic (T_d) symmetries one of which is related to the other by a 90° flipping, one obtains $8\times2=16$ states for one formula unit of $(NH_4)_3[AlF_6]$.

These two models of ionic disorder in the cubic phase predict the same entropy of transitions $\Delta S = R \ln 16 = 23.05$ J K^{-1} mol^{-1} which is in agreement with the experimental data. In addition to the symmetry argument, the NMR result favors the second model. It was pointed out that discontinuity in T_1 at the upper transition is much larger for the fluorine resonance than for the proton. One should not expect the large T_1 change in the fluorine resonance if the phase transition involved only the orientational disorder of the ammonium ions. Thus the NMR data supports the second model rather than the first.

Comparison with the Alkali Cryolites. As shown in Table 1, $(NH_4)_3[AlF_6]$ alone is cubic in the cryolite family at the room temperature. This high symmetry is a result of replacement of the spherical alkali ion by the tetrahedral ammonium ion. Three reasons may be advanced for explanation of this fact. The first is that the ammonium occupying the (1/4,1/4,1/4) position will stabilize the cubic structure. The twelve fluorine atoms surrounding the ammonium ion are grouped into four clusters of three. The four clusters, each belonging to different $[AlF_6]^{3-}$ ion, form a regular tetrahedron around the ammonium. The (1/2,0,0) ammonium and the equivalents occupy the corners of another tetrahedron which forms, together with the four aluminum atoms, the cube of the one-eighth volume of the fcc unit cell. Thus there are positive charges (NH_4^+ ions) at the four of the eight corners of the cube and negative charges (cluster of fluorine atoms) at the other four corners. The central ammonium ion will be situated stably in this tetrahedral field with its hydrogen atoms pointing toward the negative corners. Consequently, the cubic structure is stabilized by the presence of the (1/4,1/4,1/4) ammonium. This will also explain the fact that the cubic $(NH_4)_2[SiF_6]$ remains cubic at least down to 25 K:[31] the crystal has ammonium ions only in the (1/4,1/4,1/4) positions which favors the stability of the cubic lattice without orientational disorder. In alkali cryolites, the alkali ions in the (1/4,1/4,1/4) position do not offer any particular advantage for the cubic structure because the spherical alkali ions have no special reason to favor the tetrahedral environment. The structure of alkali cryolites will be dominated by the packing consideration and (at higher temperatures) by the entropy effect of the $[AlF_6]^{3-}$ disorder.

The second of the explanations for the stability of the cubic structure of the ammonium cryolite is that the orientational disorder of the (1/2,0,0) ammonium ion will decrease the free energy of the cubic phase relative to the non-cubic phase at sufficiently high temperature. Position of the (1/2,0,0) ammonium ion is not known at present. However, it will be reason-

able to suppose that orientational disorder (and decrease of the free energy) is possible only in the cubic phase, as the experimental transition entropy indicates. Such a stabilization of the cubic phase is not available to the alkali cryolites because alkali ions lack orientational degree of freedom. In passing it may be interesting to note here that $A[PF_6]$ crystals, where A is alkali or ammonium ion, are all cubic (except for Li salt) at room temperatures and undergo phase transitions at lower temperature.[1,29,30] It may be argued that orientational disorder of $[PF_6]^-$ ions stabilizes the cubic phase of these crystals.

Finally, the third of the factors contributing to the stability of the cubic ammonium cryolite is that the ionic radius of the ammonium ion may be favorable for the packing of the ions in the cubic lattice. Comparison of the unit cell dimensions of the ammonium, rubidium and caesium cryolites gives some support to this view. If we define the cubicity ratio $\gamma_c=c/(\sqrt{2}\,a)$ where a and c are unit cell lengths of the tetragonal crystal, we obtain $\gamma_c=1.0098$ for $Rb_3[AlF_6]$ and 0.9945 for $Cs_3[AlF_6]$ from the X-ray data of Holm.[32] Linear interpolation between the Rb and Cs gives $\gamma_c=1.0043$ for $(NH_4)_3[AlF_6]$ where the cubic cell dimension (0.893 nm) was taken from Steward and Rooksby.[7] The calculated cubicity ratio of the ammonium cryolite is not exactly equal but closer to the ideal cubic value 1 than the corresponding ratios of the rubidium and caesium cryolites are. Thus, it may be argued that as the size of cation increases the tetragonal cell changes from prolate to oblate and the ammonium happens to have the size that is favorable for the cubic packing. This will decrease the anisotropy of the environment of the ammonium ion and thus increase the tendency toward disordering of the ion discussed above.

We have presented triple reasons, the first energetic, second entropic and the third due to packing consideration, to explain the apparently contradictory fact that less symmetric ammonium ion forms more symmetric crystal in the cryolite family. Alkali cryolites undergo phase transition at higher temperatures.[32,33] It will be interesting to study the heat capacity of these substances to see if the orientational disorder of $[AlF_6]^{3-}$ ion proposed here will be substantiated by the experimental data for the entropy of transition.

Temperature Dependence of the Anomalous Entropy. In Fig. 9, the excess entropy $\Delta S(T)$ is plotted against the temperature. This quantity was calculated by integrating the excess heat capacity,

$$\Delta S(T) = \int^{T} \{\Delta C(T')/T'\} \cdot \mathrm{d}T'.$$

The anomalous entropy increases gradually in the intermediate phase and jumps discontinuously at the upper transition temperature to the high temperature value. Thus, the phase transition is of the first order in agreement with the T_1 discontinuity at the transition. The discontinuous part of the anomalous entropy is 13.2 J K^{-1} mol^{-1} in the total of 22.7±1.5 J K^{-1} mol^{-1}. This behavior is very similar to that observed in $(NH_4)_3[FeF_6]$[6] (discontinuity 18.5 J K^{-1} mol^{-1}, total 24.8±1.9 J K^{-1} mol^{-1}).

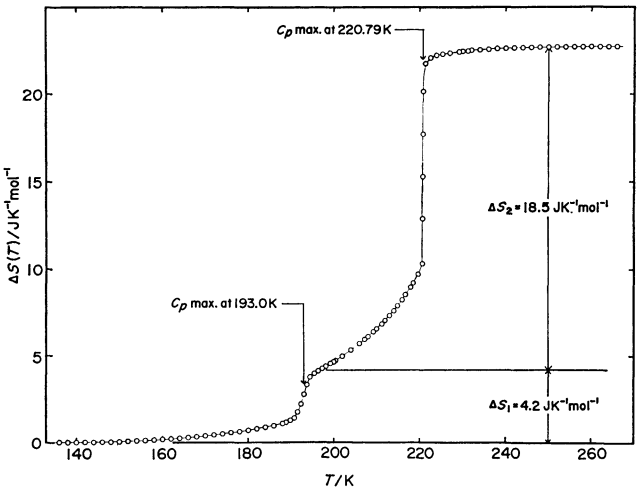

Fig. 9. Temperature dependence of the anomalous entropy $\Delta S(T)$.

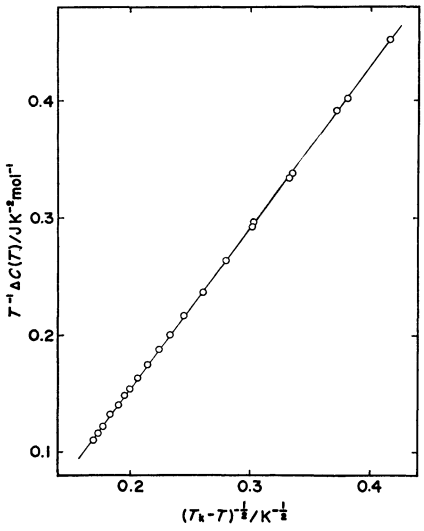

Fig. 10. $\Delta C(T)/T$ plotted against $(T-T_k)^{-1/2}$ with $T_k=224.9$ K.

The gradual increase of the entropy near the upper phase transition will be described by the Landau theory of the phase transition. The free energy of a crystal is expanded in powers of a certain order parameter.

$$G = (T-T_c)a\eta^2 + \frac{1}{2}b\eta^4 + \frac{1}{3}c\eta^6.$$

By differentiation of the free energy, one obtains the heat capacity. Figure 10 shows the plot of the anomalous encraty $(\Delta C_p/T)$ against $(T_k-T)^{-1/2}$ for $T_k=$ 224.9 K. The linearity of the plot between 190 K and 220 K is very satisfactory up to the onset of the first order transition. The parameter values derived from the best fit are as follows.

$a = 18.4$ J K^{-1} mol^{-1}, $b = -995$ J mol^{-1}, $c = 819$ J mol^{-1}.

In the lower temperature region between 180 K and 200 K of the intermediate phase where the extent of the disorder is small, the anomalous heat capacity will be expressed as

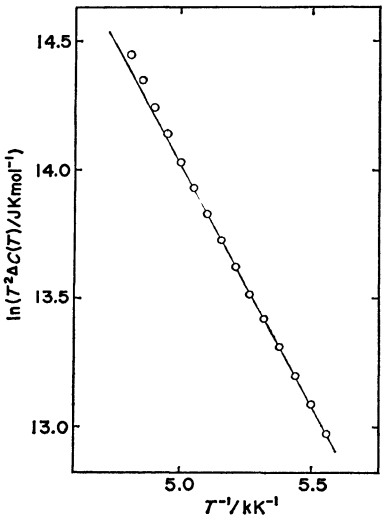

Fig. 11. $\ln(T^2\Delta C(T))$ plotted against inverse temperature.

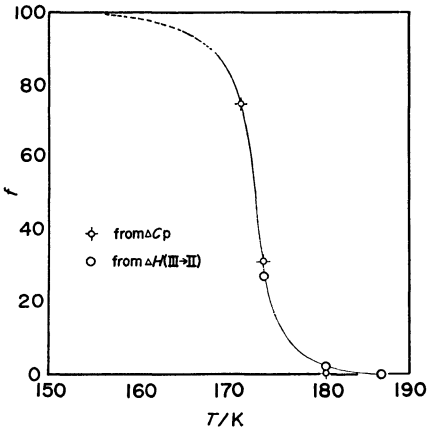

Fig. 12. Fraction of the low temperature phase *vs.* the lowest temperature to which the crystal was precooled before each measurement.

$$\Delta C(T) = R\left(\frac{\varepsilon}{RT}\right)^2 \exp[S^*/R]\cdot\exp[-\varepsilon/RT],$$

where R is the gas constant, S^* an entropic parameter (not equal to the total transition entropy and ε the molar energy required to excite the ion to the "misoriented" state in the ordered crystal. In Fig. 11, $\ln T^2\Delta C(T)$ is plotted against $1/T$. As expected the experimental heat capacity satisfies the linearity in this plot. The parameter values are $\varepsilon=15.6$ kJ mol^{-1} $S^*=51.8$ J K^{-1} mol^{-1}. In the same low temperature approximation, the anomalous entropy is given by the expression,

$$\Delta S(T) = R(\varepsilon/RT+1)\exp[S^*/R]\exp[-\varepsilon/RT].$$

By use of this equation, one can calculate the entropy which the crystal would acquire if the anomalous heat capacity of the intermediate phase continued down to zero Kelvin without being disrupted by the low temperature phase transition. $\Delta S(T=197.10\text{ K})$ calculated by this equation is equal to 2.86 J K^{-1} mol^{-1}, where the temperature 197.10 K corresponds to the minimum of the anomalous heat capacity just above the lower phase transition. The experimental value of the anomalous entropy (Fig. 9) determined by the integration of the anomalous heat capacity including that due to the lower phase transition is 3.2 J K^{-1} mol^{-1} at 197.10 K. Thus large fraction of the entropy of the lower phase transition is accounted for by the disrupted part of the upper phase transition.

It is tempting to assume that ammonium and hexafluoroaluminate ions contribute to the lower and the upper transitions separately, but the entropy of the lower transition is too small as compared with R ln 2 to support this view. At present we have no ready explanation to the fact that the phase transition in $(NH_4)_3[AlF_6]$ proceeds in two steps while the isomorphous $(NH_4)_3[FeF_6]$ has only one phase transition.

Undercooling of the Intermediate Phase. It was pointed out in the experimental section that the intermediate phase undercools and that the heat capacity of the intermediate phase was measured in its metastable temperature region. Undercooling of the present substance is very different in its character from that of typical first order transitions, *e.g.* crystallization of a simple liquid. Once the nucleation takes place in a typical undercooled liquid, the crystallization proceeds to completion consuming the liquid phase entirely, as the Gibbs phase rule dictates. In contrast, the present crystal exists in two different forms over a range of temperature. In Fig. 12, the fraction (f) of the low temperature phase is plotted against the temperature to which the crystal was cooled just before the heat capacity measurement. The measurement after precooling to 78 K gave the same heat capacity as after the precooling down to 13 K. This was taken to represent the completely transformed crystal. The fraction of the low temperature phase was calculated by two methods, one from the enthalpy of the low-temperature-to-intermediate phase transition and the other from the heat capacity difference at 184 K (see Fig. 4). The two methods gave a consistent result. A similar suspended phase change was reported in $K_4Fe(CN)_6\cdot 3H_2O$.[34] In this case, a monotropic transformation (in contrast to enantiotropic of the present crystal) from the metastable tetragonal phase to the stable low temperature phase stops in the midway depending on the temperature to which the tetragonal crystal is cooled. A simple interpretation of these anomalous metastabilities would be that slow atomic motion hinders the progress of the phase transition in these crystals. The fact that simple liquids never exhibit the anomalous metastability seems to support this interpretation because the molecular motion is certainly rapid there. However, the nuclear relaxation data presented above shows that the ionic motion is very rapid at the temperature where the under cooling of the intermediate phase occurs. Therefore the immobility of the ions cannot be the explanation of the anomalous metastability. It should be added that similar hysteresis phenomena have been reported in $Rb[PF_6]$ and $Cs[PF_6]$.[29,35] Most probably, interfacial and strain free energies caused by coexistance of the two phases will have to be taken into account for correct understanding of these phenomena.

We should like to express our best thanks to Professor Ryôichi Kiriyama, Professor Hideko Kiriyama and Dr. Masahiro Furukawa for the kind cooperation in the NMR measurement and for the fruitful discussion of the result. The X-ray powder photographs were taken with the help of Associate Professor Yôzô Chatani to whom we are grateful for his kindness. We are also indebted to Messers Masakazu Okumiya and Hiroshi Minari for the chemical analysis.

References

1) R. G. S. Morfee, L. A. K. Staveley, S. T. Walters and D. L. Wigley, *J. Phys. Chem. Solids*, **13**, 132 (1960).
2) J. Winter, K. Rossler, J. Bolz, and J. Pelzl, *Phys. Status Solidi B*, **74**, 193 (1976).
3) A. Sasane, D. Nakamura, and M. Kubo, *J. Magn. Reson.*, **3**, 76 (1970).
4) V. Novotny, C. A. Martin, R. L. Armstrong, and P. P. M. Meincke, *Phys. Rev. B*, **15**, 382 (1977).
5) Y. Furukawa, H. Kiriyama, and R. Ikeda, *Bull. Chem. Soc. Jpn.*, **50**, 1927 (1977).
6) K. Moriya, T. Matsuo, H. Suga, and S. Seki, *Bull. Chem. Soc. Jpn.*, **50**, 1920 (1977).
7) E. G. Steward and H. P. Rooksby, *Acta Crystallogr.*, **6**, 49 (1953).
8) S. Schwarzmann, *Fortschr. Mineral.*, **42**, 231 (1966).
9) The data are taken from H. Bode and E. Voss, *Z. Anorg. Allg. Chem.*, **290**, 1 (1957); D. Babel, *Structure and Bonding*, **3**, 21 (1967).
10) H. Suga, H. Chihara, and S. Seki, *Nippon Kagaku Zasshi*, **82**, 24 (1961).
11) T. Matsuo, H. Suga, and S. Seki, *J. Phys. Soc. Jpn.*, **30**, 785 (1971).
12) D. C. Look, I. J. Lowe, and J. A. Northby, *J. Chem. Phys.*, **44**, 3441 (1966).
13) Unpublished data by K. Moriya *et al.*
14) G. T. Furukawa, W. G. Saba, and J. C. Ford, *J. Res. Natl. Bur. Stand.*, **74A**, 631 (1970).
15) K. Clusius, J. Goldmann, and A. Perlick, *Z. Naturforsch., Teil A*, **4**, 424 (1949).
16) E. G. King, *J. Am. Chem. Soc.*, **79**, 2056 (1957).
17) E. Benjamins and E. F. Westrum, Jr., *J. Am. Chem. Soc.*, **79**, 287 (1957).
18) R. C. Plumb and D. F. Hornig, *J. Chem. Phys.*, **23**, 947 (1955).
19) M. Trefler and G. R. Wilkinson *Faraday Discuss. Chem. Soc.*, **48**, 108 (1969).
20) A. M. Heyns and G. J. van Schalkwyk, *Spectrochim. Acta, Part A*, **29**, 1163 (1973).
21) G. L. Cote and H. W. Thompson, *Proc. R. Soc. London, Ser. A*, **210**, 217 (1951).
22) K. S. Pitzer and W. D. Gwinn, *J. Chem. Phys.*, **10**, 428 (1942).
23) L. E. Drain, *Faraday Discuss. Chem. Soc.*, **19**, 200 (1955).
24) D. Smith, *Chem. Phys. Lett.*, **25**, 348 (1974).
25) C. A. McDowell, P. Raghunathan, and R. Srinivasan, *Mol. Phys.*, **29**, 815 (1975).
26) W. Mandema and N. J. Trappeniers, *Physica*, **76**, 102 (1974).
27) M. Guido and C. Franconi, *Ann. Chim. (Rome)*, **53**, 1048 (1963).
28) R. Blinc and G. Lahajnar, *J. Chem. Phys.*, **47**, 4146 (1967).
29) H. S. Gutowsky and S. Albert, *J. Chem. Phys.*, **58**, 5446 (1973).
30) S. Albert and H. S. Gutowsky, *J. Chem. Phys.*, **59**, 3585 (1973).
31) C. C. Stephenson, C. A. Wulff, and O. R. Lundell, *J. Chem. Phys.*, **40**, 967 (1964).
32) J. L. Holm, *Acta Chem. Scand.*, **19**, 261 (1965).
33) J. L. Holm, *Acta Chem. Scand.*, **20**, 1167 (1966).
34) M. Oguni, T. Matsuo, H. Suga, and S. Seki, *Bull. Chem. Soc. Jpn.*, **48**, 379 (1975).
35) L. A. K. Staveley, N. R. Grey, M. J. Layzell, *Z. Naturforsch., Teil A*, **18**, 148 (1963).